Deep-UV high resolution cavity ring-down spectroscopy of the Schumann–Runge bands in $^{16}O_2$ and $^{18}O_2$ at wavelengths 197–203 nm

Sandro Hannemann, Eric-Jan van Duijn, Wim Ubachs *

Laser Centre, Department of Physics and Astronomy, Vrije Universiteit, De Boelelaan 1081, 1081 HV Amsterdam, The Netherlands

Abstract

With the use of a novel titanium:sapphire laser source delivering, upon fourth harmonic generation, narrowband and tunable radiation in the deep-UV, spectroscopic studies were performed on weak Schumann–Runge bands of oxygen. Improved values for rotational and fine structure molecular parameters for the $B^3\Sigma_u^-$, $v = 0$–2 states of $^{16}O_2$ were determined, as well as values for the $v = 0$–1 states in $^{18}O_2$. Signal detection was accomplished via cavity ring-down spectroscopy.
© 2005 Elsevier Inc. All rights reserved.

1. Introduction

Spectroscopic investigation on the Schumann–Runge (SR) bands, corresponding to the $B^3\Sigma_u^- – X^3\Sigma_g^-$ system in molecular oxygen, has a long history. Brix and Herzberg [1] were first to unravel triplet fine-structure characteristics for the oxygen $^3\Sigma – ^3\Sigma$ system. Thereafter many investigations have been carried out yielding accurate information on molecular constants and dynamics of the excited rovibrational levels. The importance of the SR absorption system for the modeling of the Earth's atmosphere and its radiation budget needs no further elucidation.

The SR-system is a strongly allowed system, in fact the first dipole-allowed system in oxygen. Peculiarly, in O_2 all transitions between electronic states pertaining to the assembly of two ground state ^3P atoms are forbidden in the electric dipole approximation. However, excitation to the lowest vibrational levels in the $B^3\Sigma_u^-$ excited state is weak, due to the shift toward large internuclear separation of its potential. Particularly the $(0,0)$ band in the SR band system is extremely weak; it is a textbook example of a transition solely based on wave-function density in the classically forbidden region. It was not before 1970 that this weak $(0,0)$ band was studied [2], although the fine structure could not be resolved. In a series of investigations Yoshino and co-workers [3–10] reinvestigated the oxygen SR bands at high resolution establishing a set of molecular constants representing current knowledge on the system. For the $(0,0)$ band a band oscillator strength as small as 2.95×10^{-10} was derived. From a determination of an empirical RKR potential Franck–Condon factors were calculated that indeed give a value as low as 3.0×10^{-9} for this band [11]. The same group extended their studies from the main isotopomer $^{16}O_2$ to the less abundant $^{16}O^{18}O$ [8] and $^{18}O_2$ [9], thus providing an extensive database on the spectrum of the SR-bands.

In the present study, high-resolution spectral recordings at wavelengths near 200 nm are performed on the SR $B^3\Sigma_u^- – X^3\Sigma_g^-$ system, measuring the $(0,0)$, $(1,0)$, $(2,0)$, and $(2,1)$ bands in $^{16}O_2$ using cavity ring-down spectroscopy (CRDS) and a newly designed ultra-narrow

---

* Corresponding author. Fax: +31 20 598 7999.
  E-mail address: wimu@nat.vu.nl (W. Ubachs).

bandwidth laser system in the deep-UV. The methodical aspects of the extension of CRDS into the deep-UV wavelength region were documented before [12]; here the focus is on the spectroscopic results. Also in $^{18}O_2$ a hitherto unscanned region of the SR-bands near 200 nm was investigated. The study results in upper state vibrational level molecular constants for $v' = 0$–2 in $^{16}O_2$ and $v' = 0$–1 in $^{18}O_2$.

2. Experimental

The well-known CRDS technique is applied for an investigation of some of the Schumann–Runge bands absorbing near 200 nm. A novel-type narrow band laser system is employed that was documented before [12]. A four-mirror ring-configuration gain-switched titanium:sapphire (Ti:Sa) oscillator, which is longitudinally pumped by the output of a Q-switched frequency-doubled Nd:YAG laser (at 532 nm), is injection-seeded by the output of a continuous wave (cw) ring Ti:Sa laser. Under optimum conditions this system delivers laser pulses of 15 ns duration and of near-Fourier-transform limited bandwidth at pulse energies of up to 30 mJ after amplification in a bow-tie Ti:Sa amplifier, that is also pumped by the Q-switched Nd:YAG laser. Tuning range of the system is currently between 790–855 nm. Deep-UV radiation at frequency ω_{DUV} is produced by non-linear conversion of the infrared (IR) output (ω_{IR}) in three consecutive steps: $\omega_{blue} = 2 \times \omega_{IR}$, $\omega_{UV} = \omega_{blue} + \omega_{IR}$, and $\omega_{DUV} = \omega_{UV} + \omega_{IR}$ in three non-linear crystals (BBO) cut at appropriate angles for phase-matching. Continuous tunability of the system is $1 \, cm^{-1}$ in the IR range, so for extended spectral coverage overlapping scans have to be made.

CRDS recordings at deep-UV wavelengths were obtained using a cell of length 80 cm and a diameter of 1 cm, similar as in a previous study on one of the weaker visible band systems [13]. The optical cavity, spanning the entire cell length, is formed by two reflective mirrors with $R \approx 97\%$ in the range 197–203 nm, radius-of-curvature 50 cm, and 25 mm diameter. The recordings were performed at gas pressures in the range 30–300 mbar, where the pressure was on-line monitored on a baratron. The methods for monitoring and evaluating the CRD-transients, and retrieving the absorption spectrum were described previously [12]. Wavelength calibration was performed by using an ATOS wavelength meter on the near-IR output of the cw Ti:Sa laser. This commercial instrument consists of four internal etalons providing an accuracy of 50 MHz, which was regularly verified in our laboratory by measuring absolute wavelengths of I_2 saturation lines as described in [14]. The calibration procedures lead to an absolute accuracy of the wavelength scale better then 200 MHz or $0.006 \, cm^{-1}$ at deep-UV wavelengths.

3. Spectroscopic analysis

In Fig. 1 a typical CRD-recording of the band-head region of the SR (0,0) band of $^{16}O_2$ is displayed. The horizontal axis is derived from the simultaneous wavelength measurements by the ATOS λ-meter. The values along the vertical axis in principle represent the absolute cross sections at the specified frequencies, although no efforts are undertaken to correct for possible systematic effects, e.g., due to underestimates introduced by the analysis of the decay transients [15]. Voigt line profiles were used to determine line centers of the specific rotational components in the spectrum in a fitting analysis. The resulting transition frequencies for the six principal branches in the SR (0,0) band are listed in Table 1 as well as a few weaker lines pertaining to side-branches. The accuracy of the line positions in the (0,0) band is estimated at $0.02 \, cm^{-1}$ for most of the lines, and somewhat less accurate for some weak lines.

Similarly retrieved line positions on the SR (1,0), (2,0), and (2,1) bands in $^{16}O_2$ are listed in Tables 2–4 . The accuracies in the determination of line positions is $0.03 \, cm^{-1}$ in the (1,0) band, and $0.04 \, cm^{-1}$ in the bands probing the $v' = 2$ state. The lower accuracy is due to the increased widths in the spectra, an effect of predissociation. For $^{18}O_2$ the retrieved line positions in the (0,0) and (1,0) bands are presented in Tables 5 and 6.

The observed line positions were used to derive molecular constants for the excited state vibrational levels. The SR system corresponds to an allowed $^3\Sigma_u^- - ^3\Sigma_g^-$ transition having in total 14 rotational branches, of which six principal branches, $P_1, P_2, P_3, R_1, R_2, R_3$, four weaker branches $Q_{12}, Q_{21}, Q_{23}, Q_{32}$, and four very weak branches P_{13}, P_{31}, R_{13}, and R_{31}. These branches and the fine-structure levels involved, including $(+/-)$ and (e/f) parities are displayed in Fig. 2. Both ^{16}O and ^{18}O have
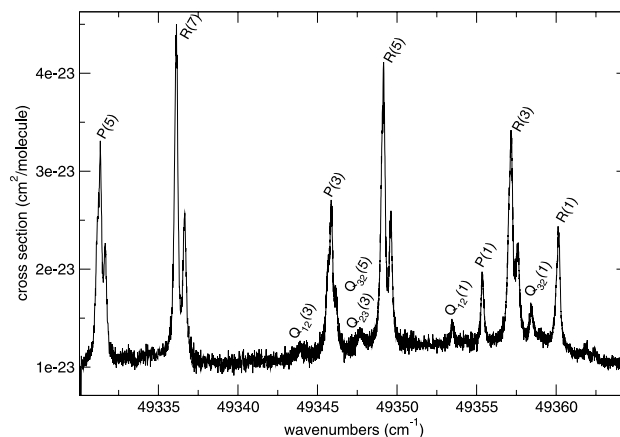

Fig. 1. Recorded spectrum by means of the CRD-method of the band head of the $B^3\Sigma_u^- - X^3\Sigma_g^-$ (0,0) band in $^{16}O_2$. In some of the lines the fine-structure splitting is readily observable.

Table 1

Observed transition frequencies for the main P and R branch lines in the $B^3\Sigma_u^- - X^3\Sigma_g^-$ (0,0) band in $^{16}O_2$ and deviations from a least-squares fit (in parentheses)

N	P_1	P_2	P_3	R_1	R_2	R_3
1	49355.368 (5)			49360.172 (−1)	49360.051 (11)	49362.424 (19)
3	49345.872 (3)	49345.653 (−11)	49346.164 (13)	49357.191 (3)	49357.052 (5)	49357.585 (−22)
5	49331.353 (1)	49331.165 (−7)	49331.662 (3)	49349.157 (−17)	49349.020 (−37)	49349.602 (−11)
7	49311.893 (5)	49311.686 (−2)	49312.662 (3)	49336.168 (14)	49336.071 (2)	49336.649 (−6)
9	49287.337 (16)	49287.221 (9)	49287.776 (6)		49318.120 (38)	49318.720 (10)
11	49257.828 (11)	49257.734 (−11)	49258.344 (−4)			
13	49223.311^b (−14)	49223.311^b (22)	49223.934 (−7)	49267.048 (−46)	49267.125 (12)	49267.831 (−3)
15	49183.851^b (4)	49183.851^b (5)	49184.543 (−4)	49234.057 (−21)	49234.152 (22)	49234.898 (−3)
17	49139.407^b (23)	49139.407^b (−11)	49184.543 (−4)	49196.064 (0)	49196.160 (12)	49196.963 (−7)
19	49089.954^b (14)	49089.954^b (−52)	49090.803 (−6)			
21	49035.576^b (60)	49035.576^b (−36)	49036.514 (47)	49105.037 (−8)	49105.193 (5)	49106.119 (6)
23	48976.136^b (22)	48976.136^b (−103)	48977.137 (−9)			

N	Q_{12}	Q_{21}	Q_{23}	Q_{32}
1	49353.481 (−5)	49361.868 (−49)		49358.464 (21)
3	49343.920 (0)		49347.707 (−41)	
5				49347.692 (91)

Blended lines are marked with b. Values in cm^{-1}.

Table 2

Observed transition frequencies for the $B^3\Sigma_u^- - X^3\Sigma_g^-$ (1,0) band in $^{16}O_2$ and deviations from a least-squares fit

N	P_1	P_2	P_3	R_1	R_2	R_3
1	50042.865 (−19)			50047.602^b (−24)	50047.602^b (12)	
3				50044.410^b (−43)	50044.410^b (0)	50044.865 (−54)
5	50018.615^b (−2)	50018.615^b (79)	50019.007 (35)	50036.130^b (−8)	50036.130^b (4)	50036.656 (27)
7	49998.791^b (−6)	49998.791^b (34)	49999.241 (19)	50022.703^b (−1)	50022.703^b (−30)	50023.262 (−5)
9	49973.875^b (4)	49973.875^b (−1)	49974.402 (20)	50004.171^b (17)	50004.171^b (−58)	50004.772 (−32)
11				49980.546^b (59)	49980.546^b (−64)	49981.253 (22)

Blended lines are marked with b. Values in cm^{-1}.

Table 3

Observed transition frequencies for the $B^3\Sigma_u^- - X^3\Sigma_g^-$ (2,0) band in $^{16}O_2$ and deviations from a least-squares fit

N	P_1	P_2	P_3	R_1	R_2	R_3
1	50707.944 (−56)			50712.665^b (−4)	50712.665^b (−4)	
3	50698.344^b (−22)	50698.344^b (51)	50698.776 (46)	50709.306^b (4)	50709.306^b (16)	50709.838 (66)
5	50683.451^b (−15)	50683.451^b (35)	50683.823 (−1)	50700.689^b (10)	50700.689^b (−5)	50701.180 (16)
7	50663.343^b (4)	50663.343^b (18)	50663.775 (18)	50686.843^b (16)	50686.843^b (−37)	50687.331 (−45)
9	50638.011^b (17)	50638.011^b (−12)	50638.497 (6)	50667.788^b (36)	50667.788^b (−60)	50668.363 (−19)
11	50607.462^b (25)	50607.462^b (−49)	50608.012 (−9)	50643.455 (−2)	50643.655 (57)	50644.203 (28)
13	50571.712^b (43)	50571.712^b (−78)	50572.349 (3)	50613.941 (−1)	50614.212 (82)	50614.778 (25)
15	50530.688 (−7)	50530.939 (76)	50531.486 (20)	50579.202 (−8)	50579.507 (62)	50580.123 (8)
17	50484.515 (−2)	450484.781 (48)	50485.451 (67)	50539.245 (−15)	50539.574 (30)	50540.300 (38)
19				50494.056 (−39)	50494.429 (1)	50495.199 (5)

N	Q_{21}	Q_{32}
1	50714.654 (108)	50711.071 (49)

Blended lines are marked with b. Values in cm^{-1}.

I = 0 nuclei and therefore the even rotational levels in the $X^3\Sigma_g^-$ ground state do not exist in the homonuclear $^{16}O_2$ and $^{18}O_2$ molecules.

For the triplet structure of the excited state we follow the analysis of Cheung et al. [6], who obtained for the F_2 levels an expression

$$E(F_2) = v_0 + Bx - Dx^2 + \tfrac{2}{3}[\lambda + (1+x)\lambda_D] - [\gamma + (1+x)\gamma_D] \tag{1}$$

using $x = J(J+1)$. Here v_0 is the vibronic band origin, B is the rotational constant, D is the centrifugal

Table 4
Observed transition frequencies for the $B^3\Sigma_u^- - X^3\Sigma_g^-$ (2,1) band in $^{16}O_2$ and deviations from a least-squares fit

N	P_1	P_2	P_3	R_1	R_2	R_3
1	49151.558 (−88)					
3				49153.081[b] (−25)	49153.081[b] (−6)	49153.495 (−74)
5	49127.516[b] (−37)	49127.516[b] (19)	49127.894 (−14)	49144.779[b] (12)	49144.779[b] (4)	49145.252 (4)
7	49107.867[b] (30)	49107.867[b] (49)	49108.325 (72)	49131.339[b] (13)	49131.339[b] (−33)	49131.870 (−2)
9	49083.024[b] (−6)	49083.024[b] (−29)	49083.529 (4)	49112.811[b] (23)	49112.811[b] (−67)	49113.411 (−5)
11	49053.165[b] (29)	49053.165[b] (−40)	49053.704 (15)	49089.144[b] (−13)	49089.144[b] (−148)	
13	49018.185[b] (25)	49018.185[b] (−89)	49018.800 (−34)	49060.488[b] (55)	49060.488[b] (−127)	49061.215 (−26)
15	48978.105[b] (2)	48978.105[b] (−160)	48978.706 (−165)	49026.599 (−18)	49026.886 (40)	49027.459 (−62)

Blended lines are marked with b. Values in cm^{-1}.

Table 5
Observed transition frequencies for the main P and R branch lines in the $B^3\Sigma_u^- - X^3\Sigma_g^-$ (0,0) band in $^{18}O_2$ and deviations from a least-squares fit

N	P_1	P_2	P_3	R_1	R_2	R_3
1	49380.309 (5)			49384.592 (−26)		
3	49371.915 (19)	49371.786 (51)	49372.223 (−3)	49381.990 (24)	49381.864 (−1)	49382.360 (−9)
5	49359.010 (13)	49358.838 (−25)	49359.304 (−7)	49374.857 (15)	49374.718 (−61)	49375.255 (−6)
7	49341.665 (17)	49341.574 (15)	49342.022 (13)	49363.245 (−24)		49363.734 (−7)
9		49319.864 (40)	49320.275 (−8)	49347.235 (−17)		49347.789 (0)
11	49293.604 (28)			49326.795 (2)		49327.398 (−1)
13				49301.909 (13)		49302.564 (−6)
15	49227.896 (12)	49227.883 (−167)	49228.543 (23)			49234.898 (−3)
17	49188.376 (8)		49189.064 (−9)	49238.786 (−4)		49239.617 (21)
19				49200.586 (1)		49201.439 (−14)
	Q_{32}					
1	49382.938 (−18)					

At the bottom of the table a single side-branch line is given. Values in cm^{-1}.

Table 6
Observed transition frequencies for the main P and R branch lines in the $B^3\Sigma_u^- - X^3\Sigma_g^-$ (1,0) band in $^{18}O_2$ and deviations from a least-squares fit

N	P_1	P_2	P_3	R_1	R_2	R_3
1	50029.548 (−26)			50033.813[b] (−22)	50033.813[b] (10)	
3				50030.993[b] (−33)	50030.993[b] (6)	50031.576 (103)
5	50008.039[b] (−18)	50008.039[b] (54)	50008.414 (0)	50023.646[b] (−6)	50023.646[b] (7)	50024.131 (13)
7	49990.457[b] (−1)	49990.457[b] (38)	49990.909 (43)	50011.723[b] (−12)	50011.723[b] (−35)	50012.250 (−12)
9	49968.339[b] (15)	49968.339[b] (15)	49968.873 (69)	49995.293[b] (15)	49995.293[b] (−48)	49995.877 (−5)
11				49974.318[b] (36)	49974.318[b] (−70)	49974.963 (−7)
13				49948.818[b] (72)	49948.818[b] (−79)	49949.549 (27)

Blended lines are marked with b. Values in cm^{-1}.

distortion parameter, λ and λ_D the spin–spin interaction parameters, and γ and γ_D the spin–rotation interaction parameters. Energies $E(F_1)$ and $E(F_3)$ levels are obtained from a diagonalization of a matrix

$$\begin{pmatrix} M_{11} & M_{12} \\ M_{21} & M_{22} \end{pmatrix} \tag{2}$$

with elements:

$$M_{11} = v_0 + B(x+2) - D(x^2 + 8x + 4) - \tfrac{4}{3}[\lambda + (x+2)\lambda_D] - 2\gamma - 4\gamma_D(x+1), \tag{3}$$

$$M_{12} = -2\sqrt{x}[B - 2D(x+1)] - \sqrt{x}\left[\gamma + \gamma_D(x+4) - \tfrac{4}{3}\lambda\right], \tag{4}$$

$$M_{22} = v_0 + Bx - D(x^2 + 4x) + \tfrac{2}{3}[\lambda + x\lambda_D] - \gamma - 3x\gamma_D, \tag{5}$$

$$M_{21} = M_{12}. \tag{6}$$

For the $X^3\Sigma_g^-$ ground state a more detailed Hamiltonian is used, following the treatment of Rouillé et al. [19]. Included are higher centrifugal distortion parameters than in the simplified treatment of the excited state given
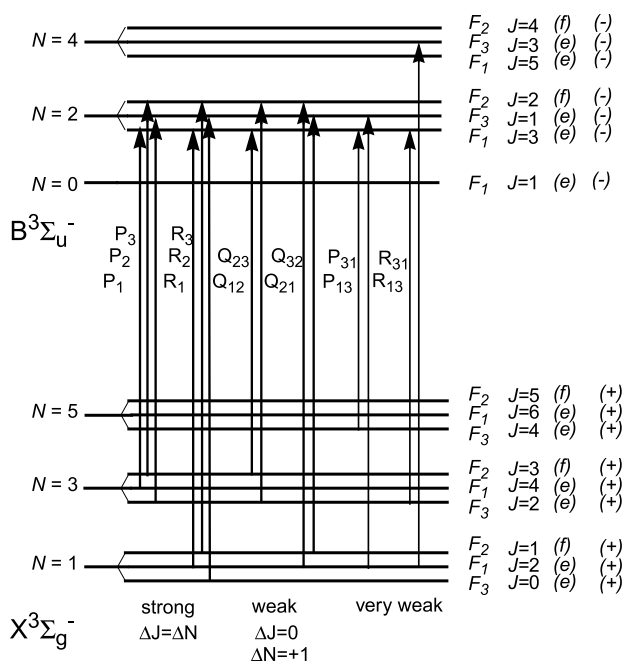
Fig. 2. Rotational branches of all allowed transitions in the $B^3\Sigma_u^- - X^3\Sigma_g^-$ system. Only the levels existing in homo-nuclear spin-0 oxygen isotopomers are shown. For clarity all $(+/-)$ and (e/f) parity assignments are given, as well as the fine-structure labels F_i, the pure rotation quantum numbers N, and the total angular momentum values J.

above. Previously, this Hamiltonian was used and verified in high-resolution studies in an analysis of a sequence of vibrational bands $(0,0)$ to $(3,0)$ in the $b^1\Sigma_g^+ - X^3\Sigma_g^-$ system [13,16–18]. Accurate constants for the ground state are determined from Raman, far-infrared and laser-magnetic-resonance data and are listed in [19] for $^{16}O_2$ for both $v = 0$ and $v = 1$ levels. These molecular constants and the ones pertaining to $^{18}O_2$, as obtained from Steinbach and Gordy [20] are listed in Table 7. In the fits these highly accurate constants are kept fixed.

Table 7
Molecular constants for the $X^3\Sigma_g^-$ ground state of oxygen for the isotopes investigated in the present study

Constant	$^{16}O_2(v=0)$	$^{16}O_2(v=1)$	$^{18}O_2(v=0)$
B	1.437676476	1.42186454	1.27800847
D	4.84256×10^{-6}	4.8418×10^{-6}	3.835×10^{-6}
H	2.8×10^{-12}	2.8×10^{-12}	
v_{10}		1556.38991	
λ	1.984751322	1.989578940	1.98459622
λ_D	1.94521×10^{-6}	2.10924×10^{-6}	1.738×10^{-6}
λ_H	1.103×10^{-11}	1.103×10^{-11}	
γ	-8.425390×10^{-3}	-8.445771×10^{-3}	-7.48648×10^{-3}
γ_D	-8.106×10^{-9}	-8.264×10^{-9}	-11.7×10^{-9}
γ_H	-4.7×10^{-14}		
Ref.	[19]	[19]	[20]

All values in cm^{-1}.

For all bands separate weighted least-squares fitting routines were performed, except for the $(2,0)$ and $(2,1)$ bands of $^{16}O_2$. In the latter case, the constants pertaining to both ground state vibrational levels $v = 0$ and $v = 1$ were kept fixed, including the separation between ground state vibrational levels v_{10}, which is more accurate in the Raman investigations [19] than in the present study. Parameters for $B^3\Sigma_u^-$, $v' = 2$ were derived from the combined fit to both sets of data. Resulting molecular constants are listed in Table 8 for $^{16}O_2$ and in Table 9 for $^{18}O_2$. The standard deviations in the fits are commensurate with the estimated uncertainties in the transitions frequencies: 0.02 cm^{-1} for $^{16}O_2$ $(0,0)$, 0.03 cm^{-1} for $(1,0)$ and 0.04 cm^{-1} for the fit of the $(2,0)$ and $(2,1)$ bands. The standard deviation in the fit for the $^{18}O_2$ $(0,0)$ band corresponds to 0.02 cm^{-1}, and for the $(1,0)$ band to 0.04 cm^{-1}. The unblended lines agree reasonably well, at the level of the estimated uncertainties, without systematic shifts. At the same time deviations between calculated and observed line positions are found for the blended lines. For example, for $J \leqslant 17$ the unresolved splitting between P_1 and P_2 components (see Table 1) causes systematic upward (P_1) and downward (P_2) shifts. Similarly the data and the deviations indicate a crossing of R_1 and R_2 components within the observed and assigned lines in the $(1,0)$ band of $^{16}O_2$ (Table 2).

In Table 8, the presently derived molecular constants are compared with those of Cheung et al. [11]. The present values for the rotational and fine-structure constants are more accurate, as a consequence of the improved resolution and frequency calibration. In the fitting procedure there is some ambiguity on the band origin. Cheung et al. [11] find a value for v_0 that is redshifted by 1.4 cm^{-1} for $^{16}O_2$. In our definition we take the trace of the Hamiltonian (the one of Rouillé et al. [19]) as the zero level for the ground state energies. The lowest energy level in the $X^3\Sigma_g^-$, $v = 0$ state is the $N = 0$, $J = 1$ level, which does not exist in the homonuclear $^{16}O_2$ molecule; it has a predicted level energy of -0.450 cm^{-1}, so below the trace of the Hamiltonian. In $^{16}O^{18}O$ this level does exist, however, at a slightly different energy [17]. In our calculation of ground state energy levels we find a non-existent $N = 0$, $J = 0$ level at 1.332 cm^{-1} for $^{16}O_2$ and at 1.331 cm^{-1} for $^{18}O_2$. Assuming that Cheung et al. [11] have taken this level as the zero for their ground state energies, and correcting for it, a genuine calibration difference of 0.10 cm^{-1} between the present result and that of Cheung et al. is left. This is reasonable in view of the resolution and the calibration procedures followed in [11]. The presently obtained value for the band origin is also in accordance with the old value of Ackerman and Baume [2] yielding $v_0 = 49358.15$ cm^{-1}.

The previous extensive work on $^{18}O_2$ by Cheung et al. [8] did not cover the $(0,0)$ and $(1,0)$ bands, hence no comparison can be made. Isotopic scaling of the rotational constants can be verified by comparing the

Table 8
Molecular constants for the $B^3\Sigma_u^-$, $v = 0$–2 states of $^{16}O_2$ as obtained from the fits

Constant	$^{16}O_2(v=0)$	Ref. [11]	$^{16}O_2(v=1)$	Ref. [11]	$^{16}O_2(v=2)$	Ref. [11]
B	0.81348 (7)	0.8132 (3)	0.7999 (2)	0.7993 (3)	0.7857 (1)	0.7860 (2)
$D \times 10^6$	4.5 (1)	4.5 (6)	6.5 (1.8)	4.2 (5)	4.5 (5)	4.4 (3)
v_0	49358.242 (6)	49358.14 (3)	50045.821 (15)	50045.70 (3)	50710.978 (9)	50710.86 (2)
λ	1.640 (7)	1.69 (3)	1.71 (2)	1.70 (3)	1.740 (7)	1.69 (2)
$\lambda_D \times 10^4$	−4.1 (1.1)					
$\gamma \times 10^2$	−3.18 (6)	−2.8 (1)	−3.51 (16)	−2.6 (1)	−3.39 (4)	−2.9 (1)
$\gamma_D \times 10^6$	2.4 (1.8)					

All values in cm^{-1}. The values for the $v = 2$ state were obtained from a simultaneous fit to the (2,0) and (2,1) bands. The values of [11] for the ground state zero level are corrected by 1.33 cm^{-1} (see text).

Table 9
Molecular constants for the $B^3\Sigma_u^-$, $v = 0$ state of $^{18}O_2$

Constant	$^{18}O_2(v=0)$	$^{18}O_2(v=1)$
B	0.7223 (3)	0.7118 (3)
$D \times 10^6$	3.1 (2)	4.5 (1.5)
v_0	49382.916 (6)	50032.237 (14)
λ	1.668 (14)	1.725 (14)
$\lambda_D \times 10^4$	20 (9)	
$\gamma \times 10^2$	−3.2 (1)	−3.28 (9)
$\gamma_D \times 10^6$	9 (4)	

All values in cm^{-1}.

rotational constants in $B^3\Sigma_u^-$, $v = 0$ for the $^{16}O_2$ and $^{18}O_2$ isotopomers, giving $B(^{18}O_2)/B(^{16}O_2) = 0.8879$ (4), which is within 2σ from the reduced mass ratio of $\mu(16)/\mu(18) = 0.8886$.

4. Conclusion

A study of the lowest vibrational levels of the $B^3\Sigma_u^-$ state in oxygen has been performed at unprecedented resolution, using a novel ultra-narrow band laser source in the deep ultraviolet and cavity ring-down absorption at these short wavelengths. Improved molecular constants have been obtained for the $v' = 0$–2 levels in $^{16}O_2$ and $v' = 0$–1 in $^{18}O_2$.

Acknowledgments

References

[1] P. Brix, G. Herzberg, Can. J. Phys. 32 (1954) 110–135.
[2] M. Ackerman, F. Biaume, J. Mol. Spectrosc. 35 (1970) 73–82.
[3] K. Yoshino, D.E. Freeman, J.R. Esmond, W.H. Parkinson, Planet. Space Sci. 31 (1983) 339–353.
[4] K. Yoshino, D.E. Freeman, W.H. Parkinson, J. Phys. Chem. Ref. Data 13 (1984) 207–227.
[5] A.S.-C. Cheung, K. Yoshino, W.H. Parkinson, D.E. Freeman, Can. J. Phys. 62 (1984) 1752–1762.
[6] A.S.-C. Cheung, K. Yoshino, W.H. Parkinson, D.E. Freeman, J. Mol. Spectrosc. 119 (1986) 1–10.
[7] K. Yoshino, D.E. Freeman, J.R. Esmond, W.H. Parkinson, Planet. Space Sci. 35 (1987) 1067–1075.
[8] A.S.-C. Cheung, K. Yoshino, D.E. Freeman, W.H. Parkinson, J. Mol. Spectrosc. 131 (1988) 96–112.
[9] A.S.-C. Cheung, K. Yoshino, D.E. Freeman, R.S. Friedman, A. Dalgarno, W.H. Parkinson, J. Mol. Spectrosc. 134 (1989) 362–389.
[10] T. Matsui, A.S.-C. Cheung, K.W.-S. Leung, K. Yoshino, W.H. Parkinson, A.P. Thorne, J.E. Murray, K. Ito, T. Imajo, J. Mol. Spectrosc. 219 (2003) 45–57.
[11] A.S.-C. Cheung, D.K.-W. Mok, Y. Sun, D.E. Freeman, J. Mol. Spectrosc. 163 (1994) 9–18.
[12] M. Sneep, S. Hannemann, E.J. van Duijn, W. Ubachs, Opt. Lett. 29 (2004) 1378–1380.
[13] H. Naus, W. Ubachs, J. Mol. Spectrosc. 193 (1999) 442–445.
[14] I. Velchev, R. van Dierendonck, W. Hogervorst, W. Ubachs, J. Mol. Spectrosc. 187 (1998) 21–27.
[15] H. Naus, I.H.M. van Stokkum, W. Hogervorst, W. Ubachs, Appl. Opt. 40 (2001) 4416–4426.
[16] H. Naus, A. de Lange, W. Ubachs, Phys. Rev. A 56 (1997) 4463–4755.
[17] H. Naus, S.J. van der Wiel, W. Ubachs, J. Mol. Spectrosc. 192 (1998) 162–168.
[18] H. Naus, K. Navaian, W. Ubachs, Spectrochim. Acta 55 (1999) 1255–1262.
[19] G. Rouillé, G. Millot, R. Saint-Loup, H. Berger, J. Mol. Spectrosc. 154 (1992) 372–382.
[20] W. Steinbach, W. Gordy, Phys. Rev. A 11 (1975) 729–731.